

Observation of electromagnetically induced Talbot effect in an atomic system with nonlinearity

Zhaoyang Zhang^{1,2}, Xing Liu², Dan Zhang^{1,2}, Jiteng Sheng³, Yiqi Zhang², Yanpeng Zhang^{2*} and Min Xiao^{1,4*}

¹*Department of Physics, University of Arkansas, Fayetteville, Arkansas 72701, USA*

²*Key Laboratory for Physical Electronics and Devices of the Ministry of Education & Shaanxi Key Lab of Information Photonic Technique, Xi'an Jiaotong University, Xi'an 710049, China*

³*Department of Physics and Astronomy, The University of Oklahoma, Norman, OK 73019, USA*

⁴*National Laboratory of Solid State Microstructures and School of Physics, Nanjing University, Nanjing 210093, China*

**Corresponding author: ypzhang@mail.xjtu.edu.cn, mxiao@uark.edu*

Abstract

We experimentally demonstrate the Talbot effect resulting from the repeatedly self-reconstruction of a spatially intensity-modulated probe field under the Fresnel near-field regime. By launching the probe beam into an optically induced atomic lattice (established by interfering two coupling fields) inside a thermal rubidium vapor cell, we can obtain an electromagnetically induced grating (EIG) on probe beam in a coherent three-level Λ -type Doppler-free atomic configuration with the assistance of electromagnetically induced transparency (EIT) window, which can modify and greatly enhance the Kerr nonlinearity near atomic resonance. The EIG patterns out of the cell can repeat the image at the output plane of the cell at integer multiples of Talbot length, which agree well with the theoretical prediction [*Appl. Phys. Lett.*, **98**, 081108 (2011)]. Such first demonstrated EIT Talbot effect in a coherent atomic system may pave a lensless and nondestructive way for imaging ultracold atoms or molecules.

The conventional Talbot effect characterized as self-imaging or lensless imaging is first implemented by launching a very small white light wave into a Fraunhofer diffraction grating and observing the images of the periodic structure at certain periodical distances named as Talbot length [1, 2]. The wide practicability and simplicity of the self-imaging process have inspired the continuous and in-depth research on Talbot effect. [3] Especially since the invention of coherent light sources, this near-field diffraction phenomenon has made great progresses not only in optics such as optical measurement [4] and optical computing [5], but also in a variety of new areas including waveguide arrays [6], parity-time symmetric optics [7], X-ray diffraction [8], Bose–Einstein condensates (BEC) [9], second harmonic generation [10], and quantum optics [11, 12]. In 2011, the Talbot effect relied on a nonmaterial electromagnetically induced grating (EIG) [13] in an atomic system is theoretically proposed to produce the self-imaging of ultracold atoms or molecules without using any sophisticated optical components [14]. Compared with the commonly used on/off-resonant absorption imaging methods [15, 16], such predicted electromagnetically induced Talbot effect (EITE) can partially maintain the advantages such as nondestructive detection and overcome the shortcoming of complicated setup during the imaging process, which may make the new imaging method have potential to become the third commonly used approach for observing ultracold atoms or molecules cloud. Further more, based on the proposed EITE, nonlocally atomic imaging scheme relied on the second-order two-photon EITE [17] and second-order self-imaging with parametric amplification four-wave mixing [18] are also theoretically predicted with promisingly practical realizability for experiment.

Also, the atomic coherence induced by coupling and probe laser beams can enhance the resonant nonlinear interaction strength in a multi-level EIT atomic configuration. [19, 20] Actually, it is investigated that the Kerr-nonlinear index of refraction current atomic configuration can be modified and greatly enhanced near atomic resonant condition, where the Kerr-nonlinear coefficient has already been directly measured. [19] Consequently, the enhanced nonlinearity is a necessary consideration during the self-imaging process.

Inspired by the promising prospect of such electromagnetically induced self-reconstruction or self-imaging effect, we experimentally demonstrate the EITE by constructing an EIG under electromagnetically induced transparency (EIT) [21, 22] condition in a three-level ^{85}Rb atomic configuration with Kerr nonlinearity. The EIG is achieved by launching a probe field into a spatially distributed optical lattice. The optically induced lattice (along the transverse direction x) inside the coherently-prepared atomic medium is generated by a resonant standing-wave coupling laser field propagating along the z direction. As a result,

we can observe the spatially intensity-modulated probe field [23] at the output plane of the vapor cell, which also implies the generation of the spatially modulated probe-field susceptibility. The manifestation of such EIT-assisted Talbot effect is concluded through the repetition of the image at the output surface of the cell at the Talbot planes. The experimentally measured axial repetition period can be very close to the calculated Talbot length d^2/λ_1 , where d and λ_1 are defined as the spatial period of the lattice and wavelength of the probe field, respectively. Although the current work is implemented in a thermal environment, the experimental demonstration can certainly be applied to ultracold atoms due to the Doppler-free spatial lights arrangement [24]. The observations might provide a promisingly new method for imaging the atomic or molecular cloud and broaden variety imaging applications such as atomic lithography [25].

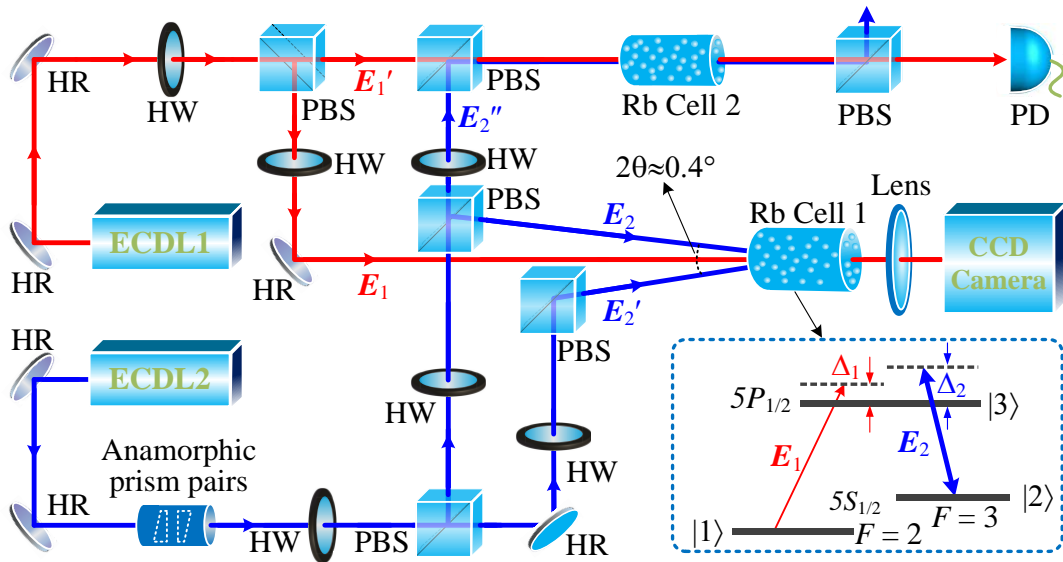


Figure 1 (color online). The experimental setup and the Λ -type energy-level configuration (in the dashed box). The output of the probe beam is imaged onto a CCD camera with a lens. Beams E_1 and E_2 are injected into the auxiliary cell2 to generate EIT window in frequency domain (detected by PD), which can monitor the frequencies of the probe and coupling lasers. ECLD: external cavity laser diode, HW: half wave plate, HR: high reflectivity mirror, PBS: polarizing beam splitter, PD: photodiode detector, CCD: charge coupled device.

The experimental setup and energy-level structure are shown in Fig. 1. The probe field E_1 (wavelength $\lambda_1=794.97$ nm, frequency ω_1 , horizontal polarization, Rabi frequency Ω_1) and the standing-wave field (established by interfering two elliptical-shaped coupling beams) propagate along the same z direction to connect a three-level Λ -type ^{85}Rb atomic system (the energy-level structure in the dashed box of Fig. 1), which is consisting of two hyperfine states $F=2$ (state $|1\rangle$) and $F=3$ (state $|2\rangle$) of the ground state $5S_{1/2}$ and one excited states $5P_{1/2}$ (state

|3>). The pair of coupling beams E_2 and E_2' ($\lambda_2=794.97$ nm, ω_2 , vertical polarization, Ω_2 and Ω_2' , respectively) from the single-mode tunable external cavity diode laser (ECDL2) are symmetrically arranged with respect to the z direction. The two coupling beams intersect at the center of Rb cell1 with an angle of $2\theta\approx 0.4^\circ$ to construct an optically induced atomic lattice along the transverse direction x when the frequency detuning Δ_2 is tuned to be near resonant with transition $|1\rangle\rightarrow|2\rangle$. Here $\Delta_i=\omega_{ij}-\omega_i$ is the detuning between the resonant transition frequency ω_{ij} and the laser frequency ω_i of E_i ($i=1, 2$). The 7.5 cm long cell1 is wrapped with μ -metal sheet and heated by the heater tape to provide an atomic density of $\sim 2.0\times 10^{12}\text{cm}^{-3}$ at 80°C . The spatial periodicity of the optically induced lattice along x direction is calculated as $d=\lambda_2/2\sin\theta\approx 114\ \mu\text{m}$.

With the near-parallel weak probe beam E_1 with an ellipse-Gaussian intensity profile from another ECDL1 launched into the induced lattice, the probe-field susceptibility can be spatially modulated under EIT condition. By carefully modifying the parameters such as frequency detuning and Rabi frequency of probe and coupling fields, EIG pattern on the probe field can be observed at the output plane of the cell, which is monitored by utilizing a CCD (charge coupled device) camera (see Fig. 1) with the assistance of a imaging lens. The Rabi frequency $\Omega_i=\mu_{ij}E_i/\hbar$ between $|i\rangle\leftrightarrow|j\rangle$, where μ_{ij} ($i, j=1, 2, 3$) is the dipole momentum and E_i is the amplitude of the electric field from E_i , can be controlled by adjusting the rotation angle of corresponding half-wave plates placed in front of the PBSs. The propagation characteristics of the spatially intensity-modulated probe field out of the cell can be imaged onto the CCD camera by moving the lens (which is placed on a precision translation stage) along the z direction. In the meanwhile, the CCD camera fixed on another translation stage is also moved to make the distance (along the z direction) between the camera and the lens constantly be equal to the twice of the focal length of the lens, which can guarantee the consistency of imaging results at different observing planes. In addition, we use the EIT technique to calibrate the position of E_2 field on the $D1$ transition line of E_1 during the experimental process, which is realized by coupling two beams E_1' and E_2'' (splitting from the above ECDL1 and ECDL2, respectively) into the second auxiliary cell2 to generate the Λ -type EIT for reference.

The key scheme for the current experiment is to periodically modulate the transmission spectrum as well as the refractive-index profile of the probe field when it propagates through the one-dimensional optical lattice. With the EIT condition satisfied in the Λ -type configuration, the atomic ensemble will modify the amplitude of probe-field profile, which

can behave the same way as an amplitude grating exert modulation on an electromagnetic wave and be expressed as EIG effect. Also, the self-Kerr-nonlinear coefficient expressed as $n_2 \propto \text{Re}[\chi^{(3)}]$ [19] can be greatly enhanced and modified in the EIT window. As a result, the susceptibility (defined as $\chi = (2N\mu_{31}/\varepsilon_0 E_1) \times \rho_{31}$) between states $|1\rangle$ and $|3\rangle$ is $\chi = \chi^{(1)} + \chi^{(3)}(|\Omega_2|^2 + |\Omega_2'|^2)$, where the linear $\chi^{(1)}$ and nonlinear $\chi^{(3)}$ are expressed respectively by

$$\chi^{(1)} = \frac{iN|\mu_{31}|^2}{\hbar\varepsilon_0} \times \frac{1}{\left(\Gamma_{31} + i\Delta_1 + \frac{|\Omega_2|^2 + |\Omega_2'|^2 + 2\Omega_2\Omega_2' \cos(2k_2x)}{\Gamma_{21} + i\Delta_2} \right)}, \quad (1)$$

and

$$\chi^{(3)} = \frac{-iN|\mu_{31}|^2}{\hbar\varepsilon_0} \times \frac{1}{\left(\Gamma_{31} + i\Delta_1 + \frac{|\Omega_2|^2 + |\Omega_2'|^2 + 2\Omega_2\Omega_2' \cos(2k_2x)}{\Gamma_{21} + i\Delta_2} \right)^2} \times (\Gamma_{21} + i\Delta_2). \quad (2)$$

In the above two equations, term $\Gamma_{ij} = (\Gamma_i + \Gamma_j)/2$ is the decoherence rate between states $|i\rangle$ and $|j\rangle$, and Γ_i is the transverse relaxation rate determined by the longitudinal relaxation time and the reversible transverse relaxation time; N is the atomic density at ground state $|1\rangle$. Further, by adopting the plane wave expansion method, the one-dimensional periodically modulated total linear and nonlinear refractive index [26, 27] can be described as

$$n(x) = n_0 + \Delta n_1 \cos(2k_2x) + \Delta n_2 \cos(4k_2x), \quad (3)$$

where n_0 is uniform refractive index being independent of the spatial periodicity; Δn_1 and Δn_2 with different spatial periodicities are the coefficients for spatially varying terms in total refractive indices. Here n_0 contains the linear part and periodicity-independent parts contributed by $\chi^{(1)}$ and $\chi^{(3)}$, both of which also contribute to Δn_1 ; and term $\Delta n_2 \cos(4k_2x)$ accounts for the nonlinear index (from $\chi^{(3)}$) inside the grating. Equation (3) gives the physical picture for the spatially modulated refractive index experienced by the probe field with the presence of the standing-wave coupling field. To precisely show the modulated results, the numerical simulation is also presented based on the pioneering theoretical proposal [14].

The transmission spectrum of the modulated probe field at the output surface of cell is

$$T(x, L) = T(x, 0) \exp(-k_1 \chi'' L/2 + ik_1 \chi' L/2), \quad (4)$$

where χ' and χ'' are the real and imaginary parts of the susceptibility χ , respectively; $T(x, 0)$ is the input profile of plane wave E_1 ; L is the length of the cell.

Considering of the periodicity of $\chi = \chi' + i\chi''$, the representation of probe transmission can

be rewritten as the form in Fourier optics. According to the Fresnel-Kirchhoff diffraction theory and the paraxial approximation [3, 14], the amplitude of the probe field at the observation plane with a distance Z to the output surface of the cell can be expressed as

$$T(X, Z) \propto \int_{-\infty}^{+\infty} T(x, L) \exp \left[ik_1 \left(Z + \frac{\xi^2}{2Z} - \frac{\xi X}{Z} + \frac{X^2}{2Z} \right) \right] d\xi, \quad (5)$$

where ζ and X represent the coordinates of the object and observation plane, respectively. Completing the integral in Eq. (5) with the Fourier series expansion of $T(x, L)$, we can obtain the conventional Talbot effect described by

$$T(x, Z) \propto \sum_{n=-\infty}^{+\infty} C_n \exp \left(-i\pi\lambda_1 n^2 Z / d^2 + i2\pi n X / d \right), \quad (6)$$

To be specific, the probe transmission with a distance of Z_T ($Z_T = md^2/\lambda_1$ is the Talbot distance with the positive integer m viewed as the self-imaging number) can repeat the amplitude at the output plane of the vapor cell with and without shifted half period $d/2$ for odd and even integers m , respectively, which is in accordance with the traditional Talbot effect. With $d = \lambda_2/2\sin\theta$ and $\lambda_1 \approx \lambda_2$ taken into consideration, we have

$$Z_T = md^2/\lambda_1 = m \times \left(\frac{\lambda_2}{2\sin\theta} \right)^2 \times \frac{1}{\lambda_1} \approx m \times \frac{\lambda_2}{(2\sin\theta)^2} = m \times 1.63 \text{ cm} \quad (7)$$

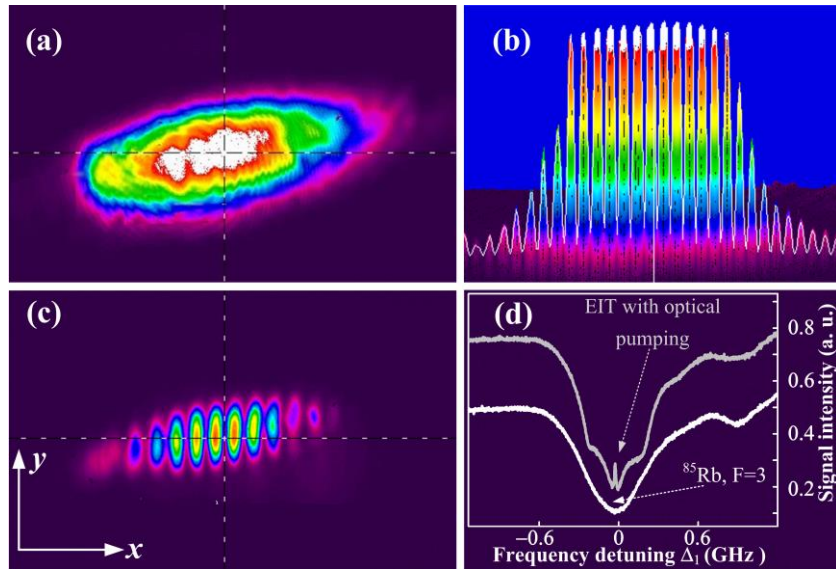


Figure 2 (color online). (a) The observed probe image. (b) The interference of the two coupling beams. (c) The experimentally generated EIG patterns on the probe field. (d) The reference EIT signal from the auxiliary cell. The upper and lower curves are the generated EIT signal and the absorption spectrum (corresponding to transition ^{85}Rb , $F=3 \rightarrow F'$), respectively.

Similarly to the theoretical derivation, the most important ingredient for the experiment

is the well establishment of spatially periodic susceptibility (namely, the optically induced atomic lattice). With the probe beam in Fig. 2(a) launched into the lattice constructed by the interference of the two coupling beams, we can observe the clear EIG shown in Fig. 2(c), where the EIT window is generated under Doppler-free condition. What is worth mentioning is that the Doppler-free condition signifies to ignore the atomic thermal motion in the warm environment. The generated interference fringes in 3-dimension view are demonstrated in Fig. 2(b). By increasing the spatial periodicity of the interference over $100\mu\text{m}$ through modifying the angle 2θ , the EIG can occur on the monitor camera. Figure 2(d) is the observed spectrum of probe field from the auxiliary Rb cell2, and the lower and upper curves represent the absorption spectra and the EIT window, respectively. Another thing to note here is that the optical pumping effect [24] can appear simultaneously with the EIT in the Λ -type system constructed by the co-propagating probe and coupling fields. Such optical pumping can increase the absorption of the probe field on $D1$ line and make the intensity of the probe transmission at $\Delta_1=\Delta_2=0$ a little weaker than the case with E_2 turned off.

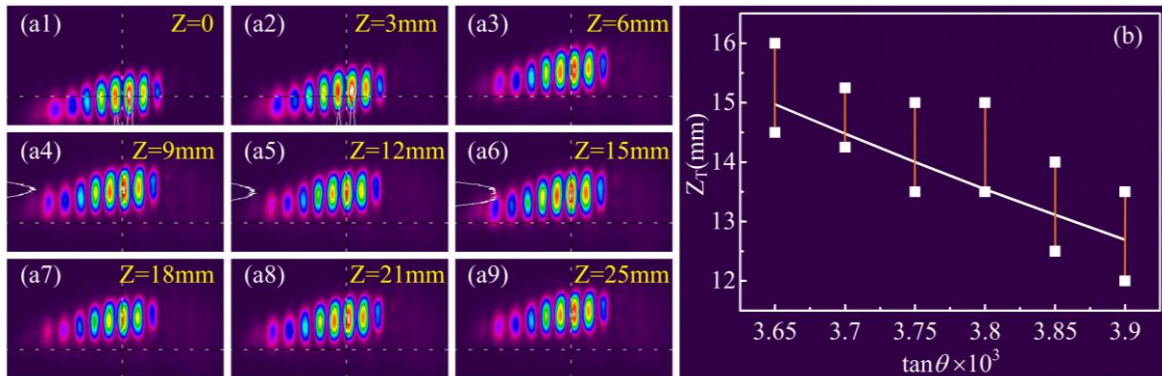


Figure 3 (color online). Demonstration of the electromagnetically induced Talbot effect. With the observation planes moving along the z direction, the intensity profile of probe field at $Z=mZ_T$ matches the profile at the output plane of cell with (m is odd integers) and without (m is even integers) shifted half a period. (j) Dependency of Talbot length on the angle between the two coupling beams. The squares are the experimental observations and the solid curve is the theoretical prediction.

With the EIG image observed at the output plane with a coordinate of $\zeta=L$, we monitor the propagation of the intensity-modulated probe beam at different observation planes. According to the previous description about the imaging lens, the CCD camera and the lens are moved with the same distance along z direction to maintain the space between them unchanged. The images at different z planes are shown in Figs. 3(a1)-(a9). According to Eq. (7), the Talbot distance is calculated as $m \times 1.63$ cm. The experimental results show that the EIG images can shift half period gradually with the observation planes tuned to $Z \approx 1.5$ cm,

which can approximately agree with the theoretical Talbot distance $Z=Z_T=1.63$ cm. When the observation coordinate exceeds $Z=1.5$ cm (the first Talbot plane, $m=1$), the EIG image can shift back to match the image at $\zeta=L$. Due to the limitation of the maximum displacement (2.5 cm) of the precision translation stage, the image at the second Talbot plane ($m=2$) is not observed. However, the moving tendency of the images at $Z=1.8$ cm, 2.1 cm and 2.5 cm can advocate that the image at $Z\approx 3$ cm will match the image at output surface of cell ($\zeta=L$) without shift. The experimental images at the first (m is odd integers) and second (m is even integers) Talbot planes can support the pioneering theoretical predictions. Also, Fig. 3(b) shows the experimentally measured evolution of Talbot length by controlling the periods of the interference fringes, which is operated by slightly varying the angle 2θ between beams E_2 and E_2' . For a given angle θ , there exists two experimental squares, which represent the EIG observed between the two Z values can keep approximately no shifting along x . Namely, the lower square (smaller Z) means the beginning coordinate where the self-reconstruction effect occurs while the upper one (larger Z) means the ending coordinate. The experimental results can basically agree with the theoretical solid curve, which advocates that the Talbot length can surely be controlled by the period of the induced lattice.

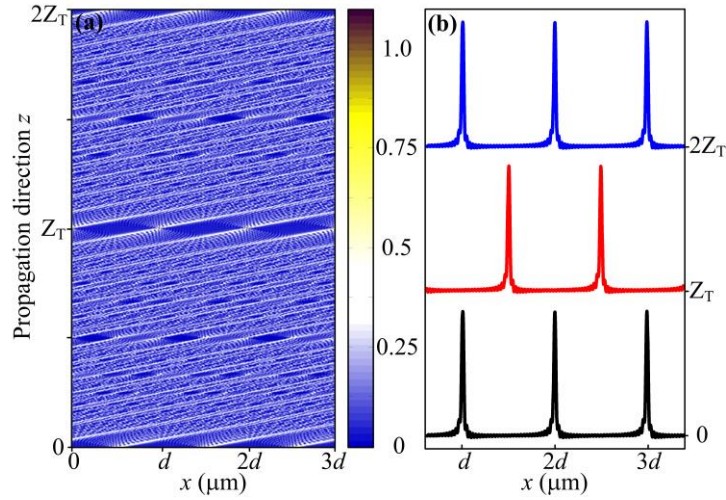


Figure 4 (color online). The calculated Talbot effect carpet for the Λ -type atomic configuration with the third-order nonlinearity considered. The dominated parameters are $\Omega_1=\Gamma_{10}$, $\Omega_2=\Omega_2'=20\Gamma_{10}$, $\Delta_1=\Delta_2=0$.

Further, we theoretically give the Talbot effect carpets as shown in Fig. 4(a) according to $\chi=\chi^{(1)}+\chi^{(3)}(|\Omega_2|^2+|\Omega_2'|^2)$ and Eq. (5). Figure 4(b) is the intensity distribution at integer Talbot distances during the self-imaging process with both $\chi^{(1)}$ and $\chi^{(3)}$ taken into consideration. By comparing Fig. 4(b) with the situation where only $\chi^{(1)}$ is considered, we find that the Talbot length are same for the both cases, which further advocates the prediction that the Talbot

distance is determined by the periodicity of the induced lattice. One thing to note is that the introduction of the large third-order nonlinearity can render the change on the intensity profile of the generated EIG as well as the self-imaging results, particularly near the resonance points where $\chi^{(3)}$ can be dramatically enhanced. Such enlarged third-order nonlinearity can be difficult to separate from the first-order susceptibility in a thermal environment, so both the linear and nonlinear processes contribute to the generation of EIG as well as Talbot effect.

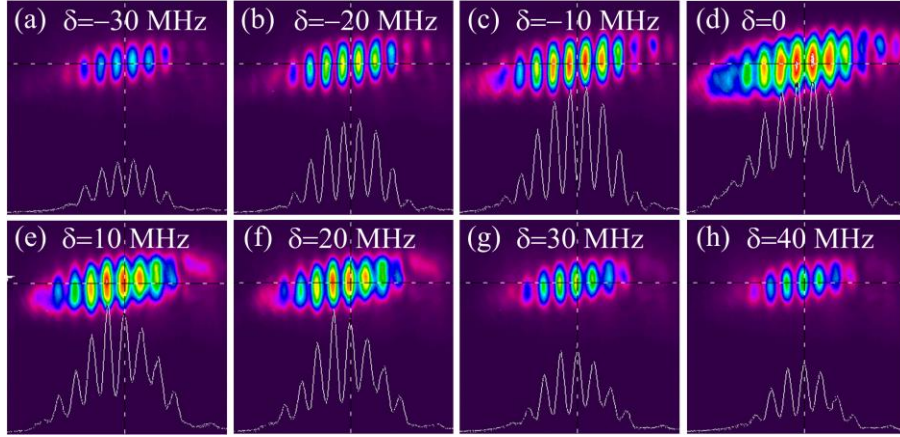


Figure 5 (color online). Experimentally observed EIG pattern versus the two-photon detuning $\delta=\Delta_1-\Delta_2$. (a) $\delta=-30$ MHz, (b) $\delta=-20$ MHz, (c) $\delta=-10$ MHz, (d) $\delta=0$, (e) $\delta=10$ MHz, (f) $\delta=20$ MHz, (g) $\delta=30$ MHz and (h) $\delta=40$ MHz, respectively.

In experiment, the nonlinearity in the periodically modulated Kerr-type atomic medium is verified by observing the spatial shift (induced by the cross-phase modulation from large refractive index modulation for probe beam) of the generated EIG. As shown in Fig. 5, with the frequency detuning of coupling field fixed at $\Delta_2=0$, the intensity of the generated EIG pattern can vary with the two-photon detuning $\delta=\Delta_1-\Delta_2$. The EIG pattern occurs the strongest at the resonant point $\delta=\Delta_1-\Delta_2=0$, while it becomes weakest at the points far away from resonance ($\delta=-30$ MHz and 40 MHz). Particularly, the EIG pattern can shift $d/2$ along the transverse x direction when the frequency detuning varies from $\Delta_1<0$ to $\Delta_1>0$ near the resonance $\Delta_1=0$. Such observed shift of the spatially intensity-modulated probe beam in a EIT medium can be attributed to the abrupt sign jump (negative \leftrightarrow positive) of the cross-Kerr nonlinear index n_2 [28]. To be specific, both terms Δn_1 and Δn_2 in Eq. (3) can be manipulated by controlling the frequency detuning Δ_1 of probe field according to the expressions in Eqs. (1) and (2). As a result, the total $n(x)$ from the sum of n_0 , $\Delta n_1 \cos(2k_2 x)$ and $\Delta n_2 \cos(4k_2 x)$ can be spatially shifted for half a period when Δ_1 jumps from negative to positive, which can also force the sign saltation of n_2 in the meanwhile. The movement means the optically induced

lattice shifts half period due to the modulation on the dispersion property and indicates that different atoms are excited. So the spatial shift can pave a way to take the images at different position of the ultracold atomic cloud by utilizing the Talbot effect without modifying the experimental setup.

In summary, the currently demonstrated EIT-assisted Talbot effect in an atomic system can provide a new and powerful methodology to image ultracold atomic or molecular cloud. Such a lensless self-imaging way may be less affected by various vibrations during practical applications. In order to simplify the experimental observation, a secondary imaging process is implemented by utilizing a convex lens with right focal length, which doesn't conflict with the advocated lensless imaging process. Moreover, although the current experiment is implemented in an EIT-medium above the room temperature, the experimental demonstration can be certainly suitable for ultracold environment with the Doppler-free effect considered. The spatial configuration of the probe field and standing-wave coupling field can meet the Doppler-free condition, which makes the observed EITE can be simulated by the theoretical model in cold atomic system without considering the thermal atomic velocity. As a consequence, the current observed EITE can be promisingly extended to ultracold environment to carry out potential applications in BEC, optical lattice and quantum information science [14].

- [1] H. F. Talbot, "Facts relating to optical science", *Philos. Mag.*, **9**, 401-407 (1836).
- [2] L. Rayleigh, "On copying diffraction gratings and on some phenomenon connected therewith", *Philos. Mag.*, **11**, 196-205 (1881).
- [3] J. M. Wen, Y. Zhang, and M. Xiao, "The Talbot effect: recent advances in classical optics, nonlinear optics, and quantum optics", *Adv. Opt. Photon.*, **5**, 83-130 (2013).
- [4] P. Xi, C. Zhou, E. Dai, and L. Liu, "Novel method for ultrashort laser pulse-width measurement based on the self-diffraction effect", *Opt. Express.*, **10**, 1009-1104, (2002).
- [5] K. Patorski, "The self-imaging phenomenon and its applications", *Prog. Opt.*, **27**, 1-108 (1989).
- [6] R. Iwanow, D. A. May-Arrioja, D. N. Christodoulides, and G. I. Stegeman, "Discrete Talbot effect in waveguide arrays", *Phys. Rev. Lett.*, **95**, 053902 (2005).
- [7] H. Ramezani, D. N. Christodoulides, V. Kovanis, I. Vitebskiy, and T. Kottos, "*PT*-Symmetric Talbot effects", *Phys. Rev. Lett.*, **109**, 033902 (2012).
- [8] F. Pfeiffer, M. Bech, O. Bunk, P. Kraft, E. F. Eikenberry, Ch. Brönnimann, C. Grünzweig, and C. David, "Hard-X-ray dark-field imaging using a grating interferometer", *Nature*

- Mater.*, **7**, 134-137 (2008).
- [9] C. Ryu, M. Andersen, A. Vaziri, M. d'Arcy, J. Grossman, K. Helmerson, and W. D. Phillips, "High-order quantum resonances observed in a periodically kicked Bose-Einstein condensate", *Phys. Rev. Lett.*, **96**, 160403 (2006).
- [10] Y. Zhang, J. M. Wen, S. N. Zhu, and M. Xiao, "Nonlinear Talbot effect", *Phys. Rev. Lett.*, **104**, 183901 (2010).
- [11] K. H. Luo, J. M. Wen, X. H. Chen, Q. Liu, M. Xiao, and L. A. Wu, "Second-order Talbot effect with entangled photon pairs", *Phys. Rev. A*, **80**, 043820 (2009).
- [12] X. B. Song, H. B. Wang, J. Xiong, K. Wang, X. D. Zhang, K. H. Luo, and L. A. Wu, "Experimental observation of quantum Talbot effects", *Phys. Rev. Lett.*, **107**, 033902 (2011).
- [13] H. Y. Ling, Y. Q. Li and M. Xiao, "Electromagnetically induced grating: Homogeneously broadened medium", *Phys. Rev. A*, **57**, 1338-1344 (1998).
- [14] J. M. Wen, S. W. Du, H. Y. Chen, and M. Xiao, "Electromagnetically induced Talbot effect", *Appl. Phys. Lett.*, **98**, 081108 (2011).
- [15] M. Andrews, C. Townsend, H. Miesner, D. Durfee, D. Kurn, and W. Ketterle, "Observation of interference between two Bose condensates", *Science*, **275**, 637-641 (1997).
- [16] L. Dobrek, M. Gajda, M. Lewenstein, K. Sengstock, G. Birkl, and W. Ertmer, "Optical generation of vortices in trapped Bose-Einstein condensates", *Phys. Rev. A*, **60**, R3381-R3384 (1999).
- [17] T. Qiu, G. Yang, and Q. Bian, "Electromagnetically induced second-order Talbot effect", *Eur. Phys. Lett.*, **101**, 44004 (2013).
- [18] F. Wen, Z. Zhang, I. Ahmed, Z. Li, H. Wang, Z. Liu, H. Gao, and Y. Zhang, "Second-order self-imaging with parametric amplification four-wave mixing", *Laser Phys. Lett.*, **13**, 075403 (2016).
- [19] H. Wang, D. Goorskey, and M. Xiao, "Enhanced Kerr nonlinearity via atomic coherence in a three-level atomic system", *Phys. Rev. Lett.*, **87**, R3381-R3384 (1999).
- [20] J. Sheng, X. Yang, H. Wu, and M. Xiao, "Modified self-Kerr-nonlinearity in a four-level N-type atomic system", *Phys. Rev. A*, **84**, 053280 (2011).
- [21] S. E. Harris, "Electromagnetically induced transparency", *Phys. Today*, **50**, 36-42 (1997).
- [22] J. Gea-Banacloche, Y. Q. Li, S. Z. Jin, and M. Xiao, "Electromagnetically induced transparency in ladder-type inhomogeneously broadened media: Theory and experiment", *Phys. Rev. A*, **51**, 576-584 (1995).

- [23] J. Sheng, J. Wang, M.-A. Miri, D. N. Christodoulides, and M. Xiao, “Observation of discrete diffraction patterns in an optically induced lattice”, *Opt. Express*, **23**, 19777-19782 (2015).
- [24] Y. Q. Li, and M. Xiao, “Electromagnetically induced transparency in a three-level Λ -type system in rubidium atoms”, *Phys. Rev. A*. **51** (4), R2703-R2706 (1992).
- [25] G. Timp, R. Behringer, D. Tennant, J. Cunningham, M. Prentiss, and K. Berggren, “Using light as a lens for submicron, neutral-atom lithography”, *Phys. Rev. Lett.* **69**, 1636-1639 (1992).
- [26] Y. Zhang, Z. Wang, Z. Nie, C. Li, H. Chen, K. Lu, and M. Xiao, “Four-wave mixing dipole soliton in laser-induced atomic gratings”, *Phys. Rev. Lett.*, **106**, 093904 (2011).
- [27] Y. Zhang, Z. Wang, H. Zheng, C. Yuan, C. Li, K. Lu, and Min Xiao, “Four-wave-mixing gap solitons”, *Phys. Rev. A*. **82**, 053837(2010).
- [28] M. Xiao, Y. Q. Li, S. Z. Jin, and J. Gea-Banacloche, “Measurement of dispersive properties of electromagnetically induced transparency in rubidium atoms”, *Phys. Rev. Lett.*, **74** (5), 666-669 (1995).